

Theoretical study of the molecular-frame photoemission time delay for K -shell photoionization of N_2

 Dmitrii V. Rezvan,¹ Nikolay M. Novikovskiy,^{1,2} Lukas Martin,¹ Anton N. Artemyev,¹ and Philipp V. Demekhin^{1,*}
¹*Institut für Physik und CINSaT, Universität Kassel, Heinrich-Plett-Strasse 40, 34132 Kassel, Germany*
²*Institute of Physics, Southern Federal University, 344090 Rostov-on-Don, Russia*


(Received 20 January 2022; accepted 2 March 2022; published 18 March 2022)

Photoelectron emission Wigner time delay for K -shell ionization of a nitrogen molecule is studied theoretically in the frame of a molecular reference for parallel and perpendicular orientations of the molecule with respect to the electric field vector of linearly polarized ionizing light. Electronic structure calculations are performed by the single center method for photoelectron kinetic energies from 5 to 20 eV and at different levels of approximation. Thereby, the influence of core relaxation effects and interchannel coupling on the $1s$ -photoemission time delays, computed across the σ^* -shape resonance, is investigated in detail. The present theoretical results can be considered as reliable predictions for future experiments.

 DOI: [10.1103/PhysRevA.105.033108](https://doi.org/10.1103/PhysRevA.105.033108)
I. INTRODUCTION

Photoionization is not an instantaneous process, since it takes typically a few to hundred attoseconds (as) to create an outgoing photoelectron wave packet which then starts leaving a system [1]. Strictly speaking, the emitted photoelectron wave is phase shifted by an ionic potential, and the electron's kinetic energy derivative of this half-scattering phase is termed the Wigner time delay [2–4]. Recent progress in the attosecond physics [5] enabled first observations of the photoemission time delays in atoms [6,7] by IR-laser field streaking or by reconstruction of attosecond beating by interference of two-photon transitions (RABBIT) techniques [8]. Since then, photoemission time delays were routinely measured in atoms and molecules [9–15]. In the case of an anisotropic potential of a molecule, the Wigner delay depends on the emission direction of the photoelectron and orientation of the light polarization with respect to the molecular axis [16]. Those theoretical predictions were first confirmed experimentally in Ref. [17] by measuring stereo time delays for parallel and perpendicular orientations of an oxygen molecule with respect to the light polarization direction.

Recent joint experimental and theoretical studies of the Wigner time delay in the inner-shell [18] and independently in the outer-shell [19] photoionization of molecules also confirmed its polarization and emission-angle dependencies. These works introduced an approach to access photoionization time delays in molecules without requiring any ultrashort pulses. It relies on the scheme of so-called *complete experiments* [20], where the amplitudes and phases of all emitted partial electron waves are extracted from the measured molecular-frame photoelectron angular distributions (MFPADs [21–24]). The multiple scattering effects, which form intricate diffraction patterns in observed MFPADs, result also in angle-dependent Wigner time delays. By scanning the

photon energy, an energy derivative of the photoelectron's phase and, as a result, the angle-dependent Wigner delay can be accessed. A theoretical study of the C K -shell photoionization of CO across the σ^* -shape resonance, performed in Ref. [18] for the $\varepsilon\sigma$ and $\varepsilon\pi$ channels, confirmed observations that the time delay in photoemission varies with respect to the emission angle within a few hundreds of attoseconds.

In the present paper, we report a theoretical study of the K -shell photoionization of the N_2 molecule. In addition to the presence of a σ^* -shape resonance in the K -shell photoionization of N_2 , an interchannel coupling between two $\varepsilon\sigma$ channels ($1\sigma_g\varepsilon\sigma_u$ and $1\sigma_u\varepsilon\sigma_g$) plays here an extremely important role [25,26]. As reported in those works, including the relaxation of the core caused by the field of a created core vacancy yields here a correct energy position of the shape resonance, while the coupling between channels results in an appearance of the shape resonance (which without coupling is present only in the $1\sigma_g\varepsilon\sigma_u$ channel) in both channels. Here, we investigate an influence of both effects on the respective angle-dependent photoemission time delays.

II. THEORY

For a linear molecule, whose axis forms an angle β with the electric field vector of linearly polarized light, the total amplitude for the emission of a photoelectron with energy ε in the direction defined by an angle θ with respect to the molecular axis is given by [18,27,28]

$$T(\varepsilon, \beta, \theta) = \sum_{\ell mk} (-i)^\ell \mathcal{D}_{k0}^1(\alpha, \beta, \gamma) A_{\varepsilon\ell mk} Y_{\ell m}(\theta, \varphi). \quad (1)$$

Here, \mathcal{D}_{k0}^1 and $Y_{\ell m}$ are the rotation matrices and spherical functions, respectively. For a parallel orientation of the molecular axis with respect to the light polarization direction, the Euler angle β is equal to 0, and for a perpendicular $\beta = \frac{\pi}{2}$. Choosing the other orientation angles $\alpha = 0$ and $\gamma = 0$ and the photoelectron emission angle $\varphi = 0, \pi$ makes the polarization and the emission planes to be the xz plane. The quantities

*demekhin@physik.uni-kassel.de

$A_{\varepsilon\ell mk}$ are the dipole transition amplitudes for the emission of the partial photoelectron continuum waves with angular momentum quantum numbers ℓ and m via the absorption of a photon of polarization k , as given in the molecular frame. The total transition amplitude (1) provides a direct access to the MFPADs and the angle-dependent Wigner time delays via [18] (atomic units are used throughout)

$$\sigma(\varepsilon, \beta, \theta) = |T(\varepsilon, \beta, \theta)|^2, \quad (2)$$

$$\tau(\varepsilon, \beta, \theta) = \frac{d}{d\varepsilon} \{\arg [T(\varepsilon, \beta, \theta)]\}. \quad (3)$$

The photoionization transition amplitudes $A_{\varepsilon\ell mk}$ were computed in the present work by the single center (SC) method and code [29,30] which was successfully applied in the past to study MFPADs of diatomic [28,31–35] and polyatomic [27,36–39] molecules.

For purposes of the present work, let us first outline the essential points of the SC method. In the method, the spatial part of a one-particle molecular orbital is represented with respect to a single molecular center as an expansion by spherical functions:

$$\Psi_\varepsilon(\mathbf{r}) = \sum_{\ell m} \frac{P_{\varepsilon\ell m}(r)}{r} Y_{\ell m}(\theta, \varphi). \quad (4)$$

In the one-channel approximation, the radial parts $P_{\varepsilon\ell m}$ satisfy a system of coupled Hartree-Fock (HF) equations [29,30]. In order to overcome difficulties in the numerical solution of those equations, caused by the nonlocal exchange interaction, we introduced the generalized spherical potentials $Y_{ckq}(r)$, which represent the harmonics of multiplicities kq of the exchange interaction of the photoelectron with all core electrons P_c [29,30]. By combining the partial radial harmonics $P_{\varepsilon\ell m}(r)$ of the photoelectron and all generalized potentials $Y_{ckq}(r)$ in the united vector solution $\bar{P}(r)$,

$$\bar{P} = \begin{pmatrix} P_{\varepsilon\ell m} \\ Y_{ckq} \end{pmatrix}, \quad (5)$$

one arrives at the following homogeneous system of coupled equations,

$$\frac{d^2\bar{P}}{dr^2} = \hat{F}\bar{P}, \quad \text{with} \quad \hat{F} = \begin{pmatrix} F_{\ell m\ell'm'} & F_{\ell mckq} \\ F_{ckq\ell'm'} & F_{ckqc'k'q'} \end{pmatrix}. \quad (6)$$

which can be solved noniteratively. Explicit expressions for the matrix \hat{F} and details on the numerical integration procedure can be found in our previous works [29,30].

In order to go beyond the one-particle HF approximation and to account for the interchannel coupling between different photoionization channels, we outline here the *multichannel* SC method (more details will be published elsewhere). Let us consider two singlet photoionization channels,

$$\begin{aligned} \nearrow \Psi^{(b\varepsilon)} &= |a^2 b^1 \varepsilon^1 \Lambda_f\rangle \\ |a^2 b^2 \Lambda_i\rangle + \omega \quad \hat{\updownarrow} \\ \searrow \Psi^{(a\varepsilon')} &= |a^1 b^2 \varepsilon'^1 \Lambda_f\rangle, \end{aligned} \quad (7)$$

which are open for ionization at the chosen photon energy ω and coupled by the following Coulomb matrix element

(includes the direct and exchange contributions):

$$\langle \Psi^{(b\varepsilon)} | \mathbf{H}^{\text{ee}} | \Psi^{(a\varepsilon')} \rangle = - \left\langle a\varepsilon \left| \frac{1}{r_{12}} \right| b\varepsilon' \right\rangle + 2 \left\langle a\varepsilon \left| \frac{1}{r_{12}} \right| \varepsilon'b \right\rangle. \quad (8)$$

This coupling can be considered as though a photoelectron emitted from one of the molecular orbitals knocks out an electron from another orbital and is itself recaptured to the original one. Combined from two solutions (5) for the $\bar{P}^{(b\varepsilon)}$ and $\bar{P}^{(a\varepsilon')}$ channels,

$$\bar{\mathbf{P}} = \begin{pmatrix} \bar{P}^{(b\varepsilon)} \\ \bar{P}^{(a\varepsilon')} \end{pmatrix}, \quad (9)$$

the coupled-channel solution $\bar{\mathbf{P}}$ satisfies a similar homogeneous system of coupled differential equations

$$\frac{d^2\bar{\mathbf{P}}}{dr^2} = \hat{\mathbf{F}}\bar{\mathbf{P}}, \quad (10)$$

with the matrix $\hat{\mathbf{F}}$ defined as

$$\hat{\mathbf{F}} = \begin{pmatrix} \hat{F}^{(b\varepsilon)} & F_{\ell m\ell'm'}^{(b\varepsilon a\varepsilon')} & F_{\ell makq}^{(b\varepsilon a\varepsilon')} \\ F_{\ell m\ell'm'}^{(a\varepsilon' b\varepsilon)} & F_{\ell mbkq}^{(a\varepsilon' b\varepsilon)} & 0 \\ 0 & 0 & \hat{F}^{(a\varepsilon')} \end{pmatrix}, \quad (11)$$

where $\hat{F}^{(b\varepsilon)}$ and $\hat{F}^{(a\varepsilon')}$ are the one-particle matrices (6) for independent channels.

As one can see from Eq. (11), the solutions for two channels (7) are coupled via direct $F_{\ell m\ell'm'}^{(b\varepsilon a\varepsilon')}$ and $F_{\ell m\ell'm'}^{(a\varepsilon' b\varepsilon)}$ and also exchange $F_{\ell makq}^{(b\varepsilon a\varepsilon')}$ and $F_{\ell mbkq}^{(a\varepsilon' b\varepsilon)}$ Coulomb interactions according to the coupling matrix element (8). Explicit analytic expressions for those interactions read

$$\begin{aligned} F_{\ell m\ell'm'}^{(b\varepsilon a\varepsilon')} &= -2 \sum_{\ell_a m_a} \sum_{\ell'_b m'_b} \sum_{kq} (-1)^{m_a+m'} \\ &\times \sqrt{(2\ell+1)(2\ell'+1)(2\ell_a+1)(2\ell'_b+1)} \\ &\times \begin{pmatrix} \ell_a & k & \ell'_b \\ 0 & 0 & 0 \end{pmatrix} \begin{pmatrix} \ell_a & k & \ell'_b \\ -m_a & q & m'_b \end{pmatrix} \\ &\times \begin{pmatrix} \ell' & k & \ell \\ 0 & 0 & 0 \end{pmatrix} \begin{pmatrix} \ell' & k & \ell \\ -m' & q & m \end{pmatrix} \\ &\times y_k(\ell_a m_a, \ell'_b m'_b), \end{aligned} \quad (12)$$

$$\begin{aligned} F_{\ell makq}^{(b\varepsilon a\varepsilon')} &= \frac{4}{r} \sum_{\ell'_b m'_b} (-1)^{m'_b} \sqrt{(2\ell+1)(2\ell'_b+1)} \\ &\times \begin{pmatrix} \ell'_b & k & \ell \\ 0 & 0 & 0 \end{pmatrix} \begin{pmatrix} \ell'_b & k & \ell \\ -m'_b & q & m \end{pmatrix} P_{\varepsilon\ell'_b m'_b}. \end{aligned} \quad (13)$$

Expressions for the couplings $F_{\ell m\ell'm'}^{(a\varepsilon' b\varepsilon)}$ and $F_{\ell mbkq}^{(a\varepsilon' b\varepsilon)}$ can be obtained from Eqs. (12) and (13) by interchanging indices $a\varepsilon'$ and $b\varepsilon$. The exchange interactions (13) couple partial photoelectron waves from each channel *only* with the generalized exchange potentials corresponding to the core orbitals being ionized in the opposite channel. The system of equations (10) can be solved by the same numerical procedure [29,30] as Eqs. (6).

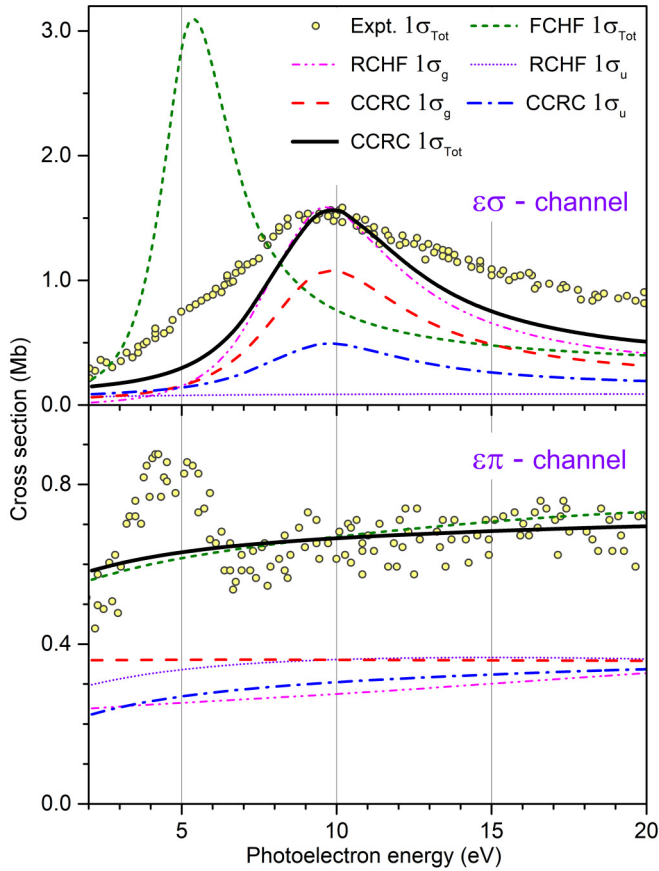


FIG. 1. The K -shell photoionization cross section of N_2 for the emission of $\varepsilon\sigma$ (upper panel) and $\varepsilon\pi$ (lower panel) partial waves. Circles: Experiment [40]. Green short-dashed curves: Frozen-core Hartree-Fock, total for $1\sigma_g$ and $1\sigma_u$ orbitals. Magenta dashed-dotted-dotted curves: Relaxed core Hartree-Fock, $1\sigma_g$ orbital. Violet short-dotted curves: Relaxed core Hartree-Fock, $1\sigma_u$ orbital. Red dashed curves: Coupled-channel relaxed core, $1\sigma_g$ orbital. Blue dashed-dotted curves: Coupled-channel relaxed core, $1\sigma_u$ orbital. Black solid curves: Coupled-channel relaxed core, total for $1\sigma_g$ and $1\sigma_u$ orbitals.

The present calculations were performed in different approximations (see below) at the equilibrium internuclear distance of N_2 using single center expansions with $\ell_c \leq 99$ and $\ell \leq 49$ for the core orbitals and for photoelectron in continuum, respectively. The energy derivative of the phase of the total transition amplitude in Eq. (3) was evaluated numerically in energy steps of 100 meV.

III. RESULTS AND DISCUSSION

A. Cross sections

Figure 1 illustrates an impact of the core relaxation and interchannel coupling on the photoionization cross sections computed for the $\varepsilon\sigma$ (upper panel) and $\varepsilon\pi$ (lower panel) channels. In the former channel, frozen-core Hartree-Fock (FCHF) calculations (green short-dashed curve in the upper panel of Fig. 1) yield the σ^* -shape resonance at a too low photoelectron energy, as compared to the experimental data (circles) from Ref. [40]. The shape resonance appears

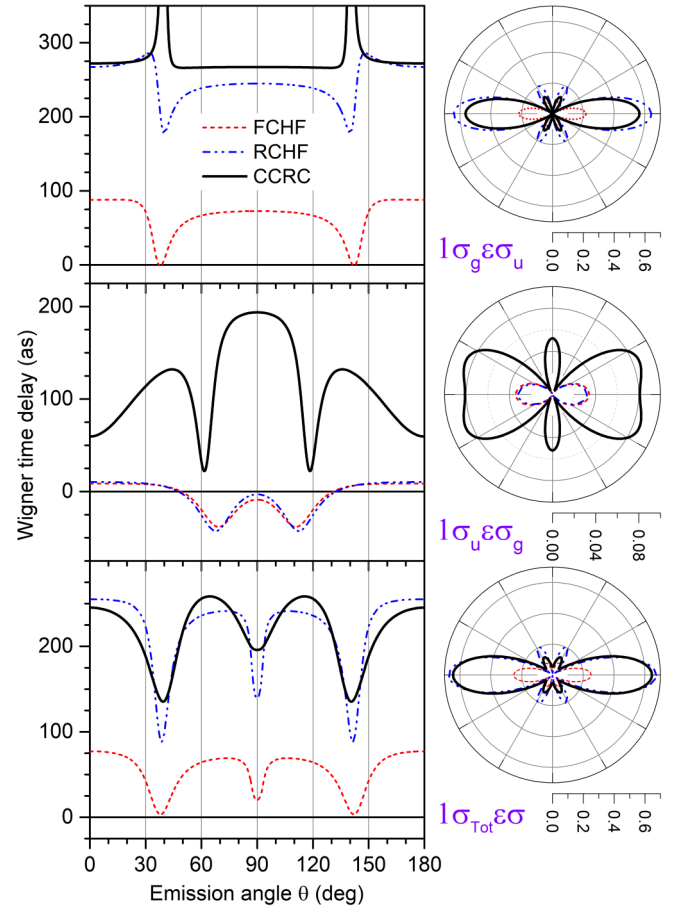


FIG. 2. The Wigner photoemission time delays (panels) and respective MFPADs (polar plots), computed at the photoelectron kinetic energy of 10 eV for the partial $1\sigma_g\varepsilon\sigma_u$ (upper row), $1\sigma_u\varepsilon\sigma_g$ (middle row), and total $1\sigma_{\text{Tot}}\varepsilon\sigma$ (lower row) channels of N_2 in different approximations (see the legend).

only in the $1\sigma_g\varepsilon\sigma_u$ channel (not shown for FCHF results). In the relaxed-core Hartree-Fock (RCHF) calculations (magenta dashed-dotted-dotted curve), this resonance manifests itself at the correct kinetic energy. Because of the interchannel coupling [coupled-channel relaxed core (CCRC) approximation], the $1\sigma_u\varepsilon\sigma_g$ channel borrows the shape resonance from the $1\sigma_g\varepsilon\sigma_u$ channel [25,26] (cf. the blue dashed-dotted and violet short-dotted curves and, separately, red dashed and magenta dashed-dotted-dotted curves in the upper panel of Fig. 1). The fact that the σ^* -shape resonance in the experimental cross section is somewhat broader than that in the computed one (cf. the circles and black solid curve) can be attributed to the vibrational broadening [25,26], which was not included in the present calculations.

Because of the absence of a shape resonance in the presently chosen photoelectron energy range, even the FCHF approximation provides a reasonable description of the $\varepsilon\pi$ channel (cf. the green short-dashed curve with circles in the lower panel of Fig. 1). Here, relaxation of the core causes only moderate changes in the total and partial cross sections (not shown for brevity). Similarly, coupling between the $1\sigma_g\varepsilon\pi_u$ and $1\sigma_u\varepsilon\pi_g$ channels (note that owing to symmetry considerations $\varepsilon\sigma$ and $\varepsilon\pi$ do not couple to each other) does not

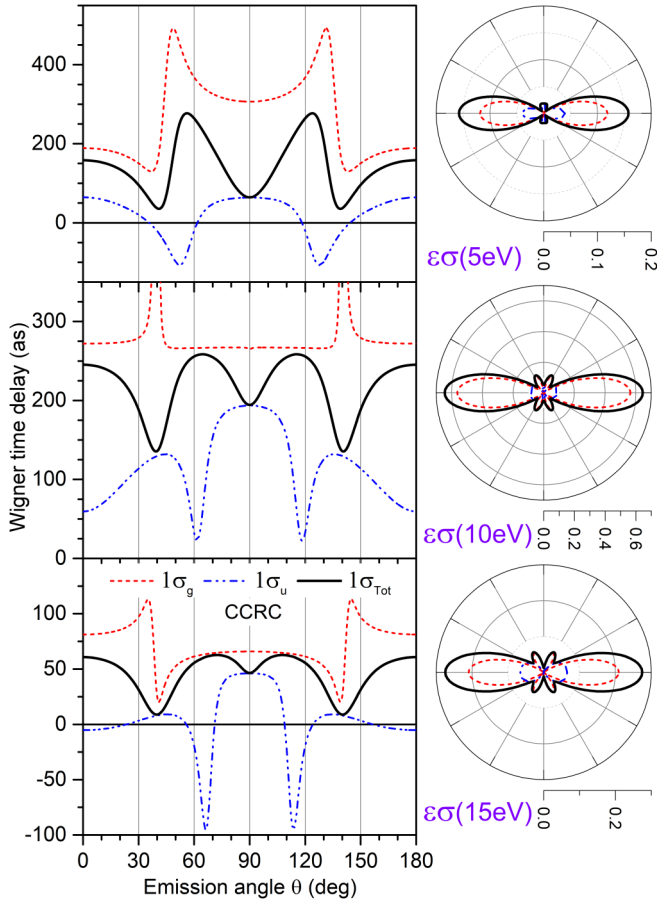


FIG. 3. The partial $1\sigma_g\varepsilon\sigma_u$, $1\sigma_u\varepsilon\sigma_g$, and total $1\sigma_{\text{Tot}}\varepsilon\sigma$ (see the legend) Wigner photoemission time delays (panels) and respective MFPADs (polar plots) of N_2 , computed for the photoelectron kinetic energies 5 eV (upper row), 10 eV (middle row), and 15 eV (lower row) in the CCRC approximation.

significantly influence the total cross section (cf. the green short-dashed and black solid curves in the lower panel). However, this coupling influences partial cross sections for these two channels and results in a swapping of their strengths in the chosen energy range (cf. the blue dashed-dotted and violet short-dotted curves and, separately, red dashed and magenta dashed-dotted curves in the lower panel of Fig. 1). As one can also see from the experimental data of Ref. [40], the photoelectron energy range below about 5 eV is strongly affected by doubly excited states, which are not included in the present theory.

B. The $\varepsilon\sigma$ channel

Figure 2 depicts the Wigner time delays and the MFPADs, computed in different approximations for the partial and total $\varepsilon\sigma$ channels and the photoelectron kinetic energy of 10 eV. For the $1\sigma_g\varepsilon\sigma_u$ partial channel (upper panel and polar plot), the FCHF approximation considerably underestimated the photoemission delay and the respective MFPAD (red short-dashed curves). This is because the chosen kinetic energy of $\varepsilon = 10$ eV lies considerably off the respective shape resonance (at about 5 eV in the FCHF approximation).

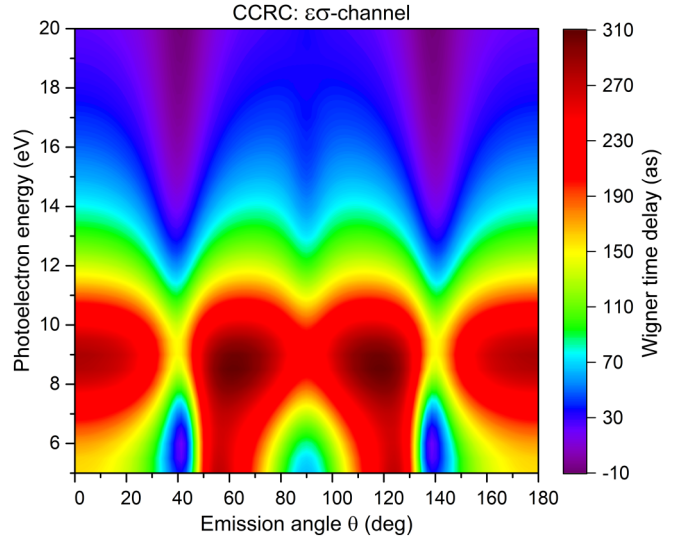


FIG. 4. The total photoemission time delay of N_2 as a function of the photoelectron kinetic energy and emission angle, computed in the CCRC approximation for the $\varepsilon\sigma$ channel.

Because this energy corresponds to the σ^* -shape resonance in the RCHF approximation, the computed MFPAD increases considerably. The same reason results in an overall increase of the computed time delay by about 200 as, since this shape resonance traps an emitted photoelectron wave inside a centrifugal barrier. The time delays (and separately MFPADs), computed for the $1\sigma_u\varepsilon\sigma_g$ channel (middle panel and polar plot of Fig. 2) are very similar. Importantly, the respective MFPADs are almost ten times smaller than for the other channel (note the scales on the respective polar plots), and the respective time delays are much smaller as well (in between -40 and 10 as).

As was pointed out in the preceding section, the inter-channel coupling shares the shape resonance between the two partial channels. Because of very different strengths of the channels, the MFPAD of the stronger $1\sigma_g\varepsilon\sigma_u$ channel decreases slightly, while that of the weaker $1\sigma_u\varepsilon\sigma_g$ channel increases considerably. The same trend applies to the computed time delays (see the black solid curves in the upper and middle panels and polar plots of Fig. 2). One should stress that photoelectron lines representing the $1\sigma_g\varepsilon\sigma_u$ and $1\sigma_u\varepsilon\sigma_g$ channels are separated by only about 100 meV [41]. Therefore, one typically observes a statistical average over the two channels. Such an averaged MFPAD is just a sum of the respective MFPADs, and the partial Wigner time delays must be weighted accordingly with the respective MFPADs:

$$\tau_{\text{Tot}}(\varepsilon, \beta, \theta) = \frac{\sum_{i=g,u} \tau_i(\varepsilon, \beta, \theta) \sigma_i(\varepsilon, \beta, \theta)}{\sum_{i=g,u} \sigma_i(\varepsilon, \beta, \theta)}. \quad (14)$$

This procedure is exemplified in Fig. 3 for the final results, obtained for the $\varepsilon\sigma$ channel in the CCRC approximation. As one can see from its middle panel and polar plot (represent data for the 10 eV photoelectron), the total (averaged) time delay oscillates between the partial time delays obtained for each channel separately: It is closer to the partial delay of a channel whose emission probability dominates at a given

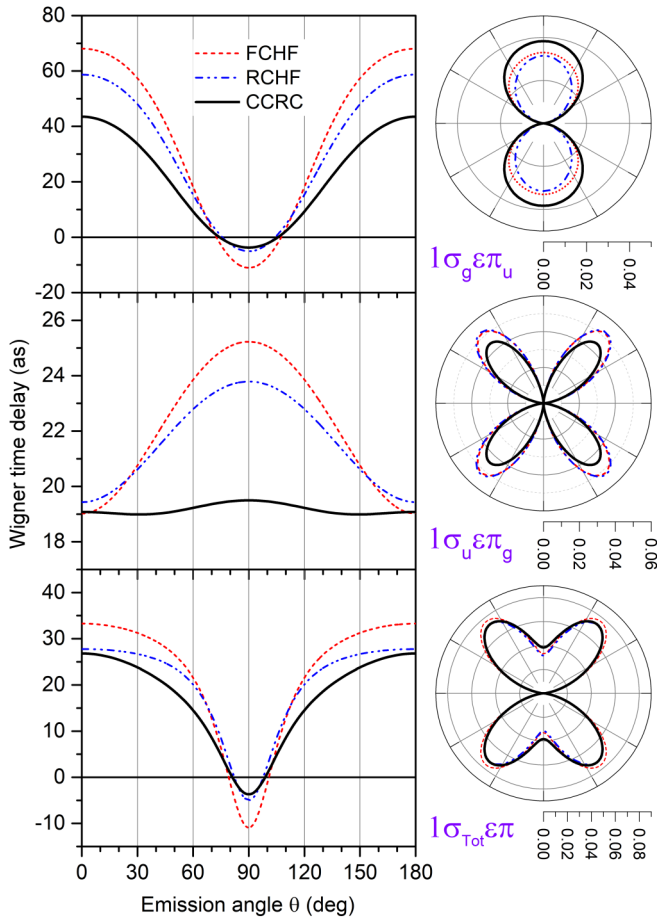


FIG. 5. The Wigner photoemission time delays (panels) and respective MFPADs (polar plots), computed at the photoelectron kinetic energy of 10 eV for the partial $1\sigma_g\varepsilon\pi_u$ (upper row), $1\sigma_u\varepsilon\pi_g$ (middle row), and total $1\sigma_{\text{Tot}}\varepsilon\pi$ (lower row) channels of N_2 in different approximations (see the legend).

emission angle θ . The lower panel and polar plot of Fig. 2 depicts such total time delays and MFPADs, computed in different approximations for the photoelectron kinetic energy of 10 eV. As one can see, the core relaxation increases the absolute values of the time delay (because of the shape resonance), while the interchannel coupling broadens dips in its angular dependence (cf. FCHF with RCHF and further with CCRC results).

Figure 3 illustrates trends in the energy dependence of the partial and total time delays and MFPADs, obtained in the CCRC approximation for the $\varepsilon\sigma$ channel. For the photoelectron energy of 5 eV, the total time delay (black solid curve in the upper panel) is large and varies as a function of the emission angle in between 30 and 270 as. Intuitively, it should decrease with the increase of the photoelectron energy, since a faster electron can easier escape the ion than a slower one. However, because of the shape resonance, the total time delay computed for the photoelectron energy of 10 eV varies in an almost similar interval of 40–260 as. For the higher kinetic energy of 15 eV (about 5 eV above the shape resonance), the total time delay drops significantly and varies in between 5 and 60 as. A complete overview of the angle-dependent time

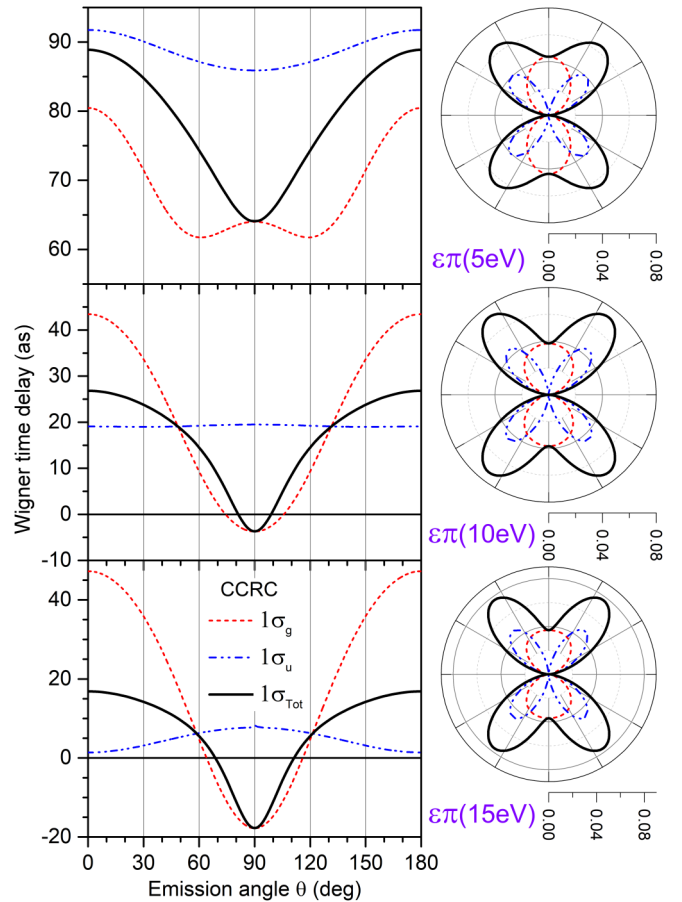


FIG. 6. The partial $1\sigma_g\varepsilon\pi_u$, $1\sigma_u\varepsilon\pi_g$, and total $1\sigma_{\text{Tot}}\varepsilon\pi$ (see the legend) Wigner photoemission time delays (panels) and respective MFPADs (polar plots) of N_2 , computed for the photoelectron kinetic energies 5 eV (upper row), 10 eV (middle row), and 15 eV (lower row) in the CCRC approximation.

delay of the $\varepsilon\sigma$ channel, computed in the CCRC approximation for the photoelectron kinetic energy range of 5–20 eV, is presented in Fig. 4. This figure supports the above-discussed trend in the energy dependence of the delay across the shape resonance and suggests that it varies in the considered energy interval with respect to the emission angle in between about -10 and 310 as.

C. The $\varepsilon\pi$ channel

Figure 5 demonstrates that relaxation of the core results in moderate changes of the partial and total Wigner time delays and MFPADs, computed for the $\varepsilon\pi$ channel at the photoelectron kinetic energy of 10 eV (cf. red dashed and blue dashed-dotted-dotted curves in each panel and polar plot). For the $1\sigma_g\varepsilon\pi_u$ channel, the interchannel coupling results in moderate changes of the time delay as well, while for the $1\sigma_u\varepsilon\pi_g$ channel, the changes are significant (cf. blue dashed-dotted-dotted and black solid curves separately in the upper panel and middle panels). These large changes in the $1\sigma_u\varepsilon\pi_g$ channel are irrelevant for the total time delay (lower panel of Fig. 5), since they take place at the emission angles around $\theta = 90^\circ$, where

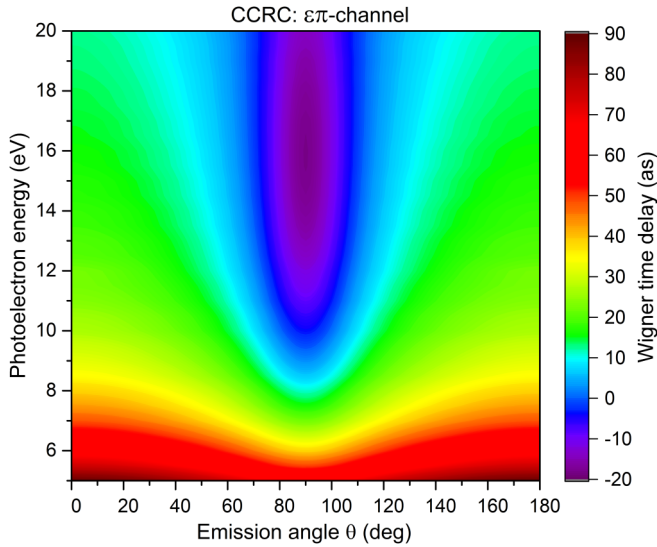


FIG. 7. The total photoemission time delay of N_2 as a function of the photoelectron kinetic energy and emission angle, computed in the CCRC approximation for the $\varepsilon\pi$ channel.

the emission probability in this channel vanishes (see the polar plot in the middle row).

Trends in the energy dependence of the partial and total time delays and MFPADs, computed for the $\varepsilon\pi$ channel in the CCRC approximation, are illustrated in Fig. 6. For the energy of 5 eV, the total time delay (black solid curve in the upper panel) is relatively large and varies with the emission angle in between 65 and 90 as. As expected, for the higher photoelectron energy of 10 eV, it drops considerably, and belongs now to the interval from -5 to 25 as (black solid curve in the middle panel). The total photoemission delay decreases

further as the photoelectron kinetic energy decreases, and for 15 eV it lies in between -20 and 20 as. As one can see from Fig. 7, which summarizes the total angle-dependent time delay computed for the $\varepsilon\pi$ channel in the CCRC approximation in the photoelectron kinetic energy range of 5–20 eV, it varies with respect to the emission angle and considered photoelectron energies in between about -20 and 90 as.

IV. CONCLUSION

Angle-dependent Wigner time delays for the K -shell photoelectron emission of the N_2 molecule are computed in different approximations for the $\varepsilon\sigma$ and $\varepsilon\pi$ channels. Calculations are performed with the single center (SC) method and code. The $\varepsilon\sigma$ channel exhibits a strong shape resonance in the considered photoelectric kinetic energy range of 5–20 eV. Therefore, the corresponding MFPADs and angle-dependent time delays are very sensitive to the level of an approximation considered in the calculations. The core relaxation and coupling between the partial $1\sigma_g\varepsilon\sigma_u$ and $1\sigma_u\varepsilon\sigma_g$ channels influences the computed time delays significantly: These effects determine not only the absolute values of the delays, but also their dependencies on the emission angle. For the $\varepsilon\pi$ channel, on the contrary, only the interchannel coupling influences the absolute values of the computed delays, without significantly changing their angular dependencies. Recent studies [18,19] provide a road map to access the presently studied angle-dependent Wigner time delay in the K -shell photoionization of N_2 by means of coincident experiments.

ACKNOWLEDGMENTS

The authors acknowledge Till Jahnke and Reinhard Dörner for many valuable discussions. This work was funded by the Deutsche Forschungsgemeinschaft (DFG) Project No. 492619011 (DE 2366/6-1).

-
- [1] R. Pazourek, S. Nagele, and J. Burgdörfer, *Rev. Mod. Phys.* **87**, 765 (2015).
- [2] L. Eisenbud, The formal properties of nuclear collisions, Ph.D. thesis, Princeton University, 1948.
- [3] E. P. Wigner, *Phys. Rev.* **98**, 145 (1955).
- [4] F. T. Smith, *Phys. Rev.* **118**, 349 (1960).
- [5] F. Krausz and M. Ivanov, *Rev. Mod. Phys.* **81**, 163 (2009).
- [6] M. Schultze *et al.*, *Science* **328**, 1658 (2010).
- [7] K. Klünder, J. M. Dahlstrom, M. Gisselbrecht, T. Fordell, M. Swoboda, D. Guenot, P. Johnsson, J. Caillat, J. Mauritsson, A. Maquet, R. Taieb, and A. L’Huillier, *Phys. Rev. Lett.* **106**, 143002 (2011).
- [8] L. Cattaneo, J. Vos, M. Lucchini, L. Gallmann, C. Cirelli, and U. Keller, *Opt. Express* **24**, 29060 (2016).
- [9] S. Heuser, A. Jimenez Galan, C. Cirelli, C. Marante, M. Sabbar, R. Boge, M. Lucchini, L. Gallmann, I. Ivanov, A. S. Kheifets, J. M. Dahlstrom, E. Lindroth, L. Argenti, F. Martin, and U. Keller, *Phys. Rev. A* **94**, 063409 (2016).
- [10] M. Huppert, I. Jordan, D. Baykusheva, A. von Conta, and H. J. Wörner, *Phys. Rev. Lett.* **117**, 093001 (2016).
- [11] M. Isinger *et al.*, *Science* **358**, 893 (2017).
- [12] S. Beaulieu *et al.*, *Science* **358**, 1288 (2017).
- [13] C. Cirelli *et al.*, *Nat. Commun.* **9**, 955 (2018).
- [14] L. Cattaneo *et al.*, *Nat. Phys.* **14**, 733 (2018).
- [15] S. Nandi *et al.*, *Sci. Adv.* **6**, eaba7762 (2020).
- [16] P. Hockett, E. Frumker, D. M. Villeneuve, and P. B. Corkum, *J. Phys. B: At., Mol. Opt. Phys.* **49**, 095602 (2016).
- [17] J. Vos, L. Cattaneo, S. Patchkovskii, T. Zimmermann, C. Cirelli, M. Lucchini, A. Kheifets, A. Landsman, and U. Keller, *Science* **360**, 1326 (2018).
- [18] J. Rist *et al.*, *Nat. Commun.* **12**, 6657 (2021).
- [19] F. Holzmeier, J. Joseph, J. C. Houver, M. Lebeck, D. Doweck, and R. R. Lucchese, *Nat. Commun.* **12**, 7343 (2021).
- [20] H. Kleinpoppen, B. Lohmann, and A. N. Grum-Grzhimailo, *Perfect/Complete Scattering Experiments* (Springer, New York, 2013).
- [21] A. Landers, T. Weber, I. Ali, A. Cassimi, M. Hattass, O. Jagutzki, A. Nauert, T. Osipov, A. Staudte, M. H. Prior, H. Schmidt-Böcking, C. L. Cocke, and R. Dörner, *Phys. Rev. Lett.* **87**, 013002 (2001).
- [22] T. Jahnke, T. Weber, A. L. Landers, A. Knapp, S. Schössler, J. Nickles, S. Kammer, O. Jagutzki, L. Schmidt, A. Czasch, T.

- Osipov, E. Arenholz, A. T. Young, R. Díez Muiño, D. Rolles, F. J. Garcia de Abajo, C. S. Fadley, M. A. Van Hove, S. K. Semenov, N. A. Cherepkov, J. Rösch, M. H. Prior, H. Schmidt-Böcking, C. L. Cocke, and R. Dörner, *Phys. Rev. Lett.* **88**, 073002 (2002).
- [23] J. B. Williams, C. S. Trevisan, M. S. Schöffler, T. Jahnke, I. Bocharova, H. Kim, B. Ulrich, R. Wallauer, F. Sturm, T. N. Rescigno, A. Belkacem, R. Dörner, T. Weber, C. W. McCurdy, and A. L. Landers, *Phys. Rev. Lett.* **108**, 233002 (2012).
- [24] H. Fukuzawa *et al.*, *J. Chem. Phys.* **150**, 174306 (2019).
- [25] N. A. Cherepkov, S. K. Semenov, Y. Hikosaka, K. Ito, S. Motoki, and A. Yagishita, *Phys. Rev. Lett.* **84**, 250 (2000).
- [26] S. K. Semenov and N. A. Cherepkov, *Phys. Rev. A* **66**, 022708 (2002).
- [27] L. Kaiser *et al.*, *J. Phys. B: At., Mol. Opt. Phys.* **53**, 194002 (2020).
- [28] G. Kastirke, M. S. Schöffler, M. Weller, J. Rist, R. Boll, N. Anders, T. M. Baumann, S. Eckart, B. Erk, A. De Fanis, K. Fehre, A. Gattton, S. Grundmann, P. Grychtol, A. Hartung, M. Hofmann, M. Ilchen, C. Janke, M. Kircher, M. Kunitski *et al.*, *Phys. Rev. X* **10**, 021052 (2020).
- [29] Ph. V. Demekhin, A. Ehresmann, and V. L. Sukhorukov, *J. Chem. Phys.* **134**, 024113 (2011).
- [30] S. A. Galitskiy, A. N. Artemyev, K. Jänkälä, B. M. Lagutin, and Ph. V. Demekhin, *J. Chem. Phys.* **142**, 034306 (2015).
- [31] H. Sann, C. Schober, A. Mhamdi, F. Trinter, C. Müller, S. K. Semenov, M. Stener, M. Waitz, T. Bauer, R. Wallauer, C. Goihl, J. Titze, F. Afaneh, L. P. H. Schmidt, M. Kunitski, H. Schmidt-Böcking, P. V. Demekhin, N. A. Cherepkov, M. S. Schöffler, T. Jahnke, and R. Dörner, *Phys. Rev. Lett.* **117**, 263001 (2016).
- [32] A. Mhamdi, J. Rist, D. Aslitürk, M. Weller, N. Melzer, D. Trabert, M. Kircher, I. Vela-Pérez, J. Siebert, S. Eckart, S. Grundmann, G. Kastirke, M. Waitz, A. Khan, M. S. Schöffler, F. Trinter, R. Dörner, T. Jahnke, and P. V. Demekhin, *Phys. Rev. Lett.* **121**, 243002 (2018).
- [33] G. Kastirke, M. S. Schöffler, M. Weller, J. Rist, R. Boll, N. Anders, T. M. Baumann, S. Eckart, B. Erk, A. De Fanis, K. Fehre, A. Gattton, S. Grundmann, P. Grychtol, A. Hartung, M. Hofmann, M. Ilchen, C. Janke, M. Kircher, M. Kunitski *et al.*, *Phys. Rev. Lett.* **125**, 163201 (2020).
- [34] A. Mhamdi, J. Rist, T. Havermeier, R. Dörner, T. Jahnke, and Ph. V. Demekhin, *Phys. Rev. A* **101**, 023404 (2020).
- [35] A. Pier, K. Fehre, S. Grundmann, I. Vela-Pérez, N. Strenger, M. Kircher, D. Tsitsonis, J. B. Williams, A. Senftleben, T. Baumert, M. S. Schöffler, P. V. Demekhin, F. Trinter, T. Jahnke, and R. Dörner, *Phys. Rev. Research* **2**, 033209 (2020).
- [36] M. Tia *et al.*, *J. Phys. Chem. Lett.* **8**, 2780 (2017).
- [37] G. Nalin *et al.*, *Phys. Chem. Chem. Phys.* **23**, 17248 (2021).
- [38] K. Fehre, N. M. Novikovskiy, S. Grundmann, G. Kastirke, S. Eckart, F. Trinter, J. Rist, A. Hartung, D. Trabert, C. Janke, G. Nalin, M. Pitzer, S. Zeller, F. Wiegandt, M. Weller, M. Kircher, M. Hofmann, L. P. H. Schmidt, A. Knie, A. Hans *et al.*, *Phys. Rev. Lett.* **127**, 103201 (2021).
- [39] K. Fehre *et al.*, [arXiv:2101.03375](https://arxiv.org/abs/2101.03375).
- [40] E. Shigemasa, K. Ueda, Y. Sato, T. Sasaki, and A. Yagishita, *Phys. Rev. A* **45**, 2915 (1992).
- [41] U. Hergenhahn, *J. Phys. B: At., Mol. Opt. Phys.* **37**, R89 (2004).